International Journal of Science and Research (IJSR)
ISSN (Online): 2319-7064
Index Copernicus Value (2013): 6.14 | Impact Factor (2013): 4.438

Microwave Analysis and Electrical Properties of ZnO thin Films Prepared by RF Magnetron Sputtering

R. Ondo-Ndong[1] Z. H. Moussambi Membetsi[2], H. Gnanaga[3], H. M. Omanda[4] and A. Foucaran[5]

[1,2,3,4] Laboratoire pluridisciplinaire des sciences, Ecole Normale Supérieure, B.P 17009 Libreville, GABON
[5]Institut Electronique du Sud, IES-Unité mixte de Recherche du CNRS n° 5214, Université Montpellier II, Place E. Bataillon, 34095 Montpellier cedex 05- FRANCE.

Abstract: ***A piezoelectric thin film sandwiched between two metal electrodes is basic structure for high frequency bulk acoustic wave device have been investigated. The films used for acoustic wave devices require high dielectric properties, piezoelectric coefficients and high electromechanical coupling coefficients, because the piezoelectric films launch and receive the acoustic wave. We fabricated ZnO films by RF magnetron sputtering. For that propose, the RF magnetron sputtering deposition for piezoelectric ZnO films formation and its such application for film bulk acoustic resonator (FBAR) devices are presented. Several critical parameters of the RF magnetron sputtering process deposition pressure, RF power, substrate temperature, O_2 concentration and the target to substrate distance were determined to clarify their effects on the material characteristics of the ZnO. Highly c-axis oriented thin films as thick as 3.8µm were grown and analyzed. Compressive stresses were observed. The FBAR devices with the ZnO films exhibited a pronounced resonance peak centred at 537 MHz with a k^2 coupling coefficient of 7 %. It found therefore that the impedance matching of the FBAR could be easily achieved simply by controlling the resonance the resonator.***

Keywords: ZnO; FBAR; R.F sputtering magnetron; resonator; electromechanical coupling coefficient

1. Introduction

The upcoming needs for higher carrier frequencies in MEMS devices, open opportunities for bulk acoustic wave (BAW) technology based on piezoelectric thin films. In particular, the need for high performance filters has become increasingly apparent as spectrum crowding increases. The Film Bulk Acoustic Resonator (FBAR) is prime candidate for the next-generation mobile communication devices to replace dielectric and surface acoustic wave (SAW) filters[1-3]. The Film Bulk Acoustic Resonator (FBAR) have become one of the most promising components, mainly due to their small size, high device performance and strong potential for the realization of microwave monolithic integrated circuits (MMIC). The most critical factor determining the resonance characteristics of FBAR devices is piezoelectric properties of the ZnO films, which is directly related to degree of the preferred orientation of the Zno crystal structure [4-5]. Considerable effort has been made to fabricate high quality ZnO films with a strongly preferred orientation. However, each approach has shown its own limitations such as the complexity of the fabrication methods and the high cost of process equipment. Various materials are used in piezoelectric devices. Among them, ZnO has a hexagonal Wurzite structure and various characteristics such as a large piezoelectric constant and an electromechanical coupling coefficient. There have been many studies on piezoelectric thin films devices and their physical properties using ZnO thin films [6-8]. Several growth techniques, such as, spray pyrolysis, sputtering, pulsed laser deposition, MBE and MOCVD have been extensively used for the deposition of un-doped and doped ZnO thin films, among which, sputtering has been the most widely used. This paper presents the resistivity properties and the analysis of ZnO based FBAR's that are centred at frequencies ranging from 500 to 600MHz. The texture of ZnO thin film was analyzed by X-ray diffraction and the electromechanical coupling coefficient k^2 was measured with Network analyzer. On the other hand the electrical properties of the resonators were measured and are discussed as function of materials parameters and processing conditions.

2. Experiment Descriptions

Zinc oxide films were deposited by r.f magnetron sputtering using a zinc target (99,99%) with diameter of 51 mm and 6 mm thick. Substrate is p-type silicon with (100) orientation. The substrates were thoroughly cleaned with organic. Magnetron sputtering was carried out in oxygen and argon mixed gas atmosphere by supplying r.f power at a frequency of 13.56 MHz. The RF power was about 50 W. The flow rates of both the argon and oxygen were controlled by using flow meter (ASM, AF 2600). The sputtering pressure was maintained at $3.35.10^{-3}$ torr controlling by a Pirani gauge. Before deposition, the pressure of the sputtering system was under 4.10^{-6} torr for more than 12 h and were controlled by using an ion gauge controller (IGC – 16 F). Thin films were deposited on silicon, substrate under conditions listed in Table1 [9]. These deposition conditions were fixed in order to obtain the well-orientation zinc oxide films.

Table 1: ZnO sputtering conditions

Sputtering pressure	3.35×10^{-5} Torr
Mixture gas	$A_r + O_2$ = 80 – 20 %
Power RF	50 W
Sputtering time	6 h
Substrate temperature	100 °C
Target-substrate distance	7 cm

Licensed Under Creative Commons Attribution CC BY

The presputtering occurred for 30min to clean the target surface. Deposition rates covered the range from 0.35 to 0.53 μm/h. All films were annealed in helium ambient at 650°C for 15mn.

In order to investigate the crystallographic properties of the ZnO films, we carried out an X-ray diffraction (XRD) analysis using CuK_α (λ = 0,154054 nm) radiation. The root-mean-square (rms) surface roughnesses of the films were characterized by using an atomic force microscope (AFM). The dielectric properties of Zno films were measured with an impedance analyzer. Typical values for the relative permittivity and the dielectric losses were 8.5 and 0.002 respectively.

Measurements of conductivity microwave are performed using an impedance analyzer HP-4192A LCR. This device provides capacity and conductance in the frequency range from 10kHz to 10MHz. The measurement principle is based on the four terminal method. An oscillator injects a current through the sample, then we measure, at its terminals, the voltage drop observed. This allows us to deduce the complex impedance. Through its compensation system, which takes into account any possible interference component, this device provides high accuracy 0.1%. The acquisition and processing of data are managed entirely by computer. Electric constants are determined under empty. The sample is fixed on a surface of the heating plate whose temperature can be controlled in the range 25°C to 300°C. The heat exchange is promoted by the bonding of the sample on the oven with a thermal adhesive.

A vacuum calibration is performed to account for the parasitic capacity links. The temperature-controlled by a PID is automatically measured by a thermocouple [chromel-alumel]. To appreciate the nature of our piezoelectric ZnO layers, we determined the coupling coefficient of the complete structure based on frequencies for which the conductance is maxima and the minima susceptance using a network analyzer (HP 8752 A Network Analyzer) whose pass-band ranges from 300 KHz to 1.3 GHz. This type of device is one of instruments to define with precision the characteristics of an electric circuit (impedance measurement, electrical admittance, reflection coefficient ...).

3. Results and discussions

3.1 A.C. Conductivity

The system combines the sample and the electrodes are treated as an equivalent circuit. Generally, it is to provide a capacitor wherein the sample plane acts as the dielectric when an alternating voltage is applied across the dielectric, an alternating current I flows, and is equal to:

$$I = i\omega\varepsilon_r C_0 V \quad (1)$$

where: ε_r is the relative permittivity and C_0 ability in the air if the dielectric is assumed to be perfect. As shown in this relationship, the current is phase shifted with respect to the voltage and the average power is zero.

In general, there is a component in phase with the voltage corresponding to "leakage current" which is entirely due to the dielectric material and is part of its properties. It is characterized by an additional component ε_r, by setting:

$$\varepsilon_r = \varepsilon_1 + i\varepsilon_2 \quad (2)$$

The total current through the circuit becomes:

$$I = I_1 + I_2 = i\omega(\varepsilon_1 + i\varepsilon_2)C_0 V = \left(iC\omega + \frac{1}{R}\right)V$$

$$\text{Either } R = \frac{1}{\varepsilon_2 C_0 \omega} \text{ and } C = \varepsilon_1 C_0 = \varepsilon_0 \varepsilon_1 \frac{A}{d} \quad (3)$$

where: d is the thickness of the dielectric layer and the surface A of dot.

Measuring magnitudes C and R e1 respectively provides $\varepsilon_1(\omega)$ (w) and $\varepsilon_2(\omega)$.

It is noted that the capacitive properties correspond to the real part of the permittivity, while $\varepsilon_2(\omega)$ dielectric properties are related to the conductance system.

By convention, it involves the loss angle, phase difference between the current I_2 loss and quadrature component I_1:

$$\tan\delta = \varepsilon_2 / \varepsilon_1 \quad (4)$$

These losses is characterized by introducing the concept of dielectric conductivity by the equation:

$$\sigma(\omega) = \varepsilon_0 \varepsilon_1 \tan\delta \quad (5)$$

The contact surface is a very important factor in achieving MEMS. Indeed, when making contact, we must minimize the risk of short circuits MIM structure (Metal-Insulator-Metal) that make the structure unusable. However, the larger the surface of the upper electrode, the greater the probability of short-circuit increases. In order to limit the short-circuit during the electrical testing thereof were carried out with the upper electrodes of circular diameter of 0.5mm, which represents a contact area of $0.2mm^2$. Once this precaution, we make measurements of the local capacity and dielectric loss under vacuum, depending on the frequency and temperature.

The electrical conductivity was determined from the loss angle: $\tan(\delta) = \frac{1}{2\pi f C_p R_p}$

where f is the frequency measured in Hz, C_P and R_P are respectively the capacitance and resistance in parallel. The conductivity σ is connected to the geometry of the sample by the equation: $\sigma = \frac{d}{R_p A}$ where A is the area of contact and d the layer thickness.

From the above two equations, we obtain the relationship of the conductivity in the form:

$\sigma = \frac{2\pi f d C_p \tan(\delta)}{A}$ We studied the a.c conductivity of the sample scheme according to the frequency in the temperature range 40°C - 250°C. Fig.1 shows the results. We will discuss these results on the basis of conduction models developed by Elliott [10].

Licensed Under Creative Commons Attribution CC BY

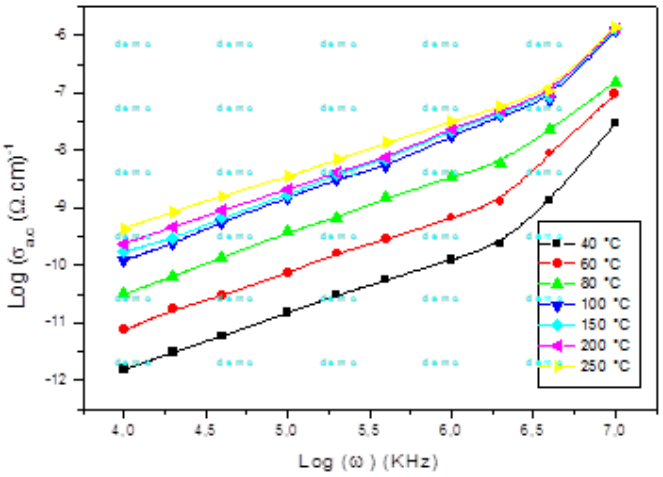


Figure 1: Typical variation of the total conductivity with frequency measured at different temperatures for sample grown at 100°C.

It appears that the more we go up in temperature, the higher the conductivity becomes independent of frequency in the low frequency range. At high frequencies, $\sigma(\omega)$ is practically independent of temperature. The conductivity is thermally activated. At high temperature, $\sigma(\omega)$can be deconvoluted into two components according to the equation: $\sigma(\omega) = \sigma_{dc} + A\omega^{s}$. The alternating component of the total conductivity is predominant at high frequency and / or low temperature. Previous studies of ZnO thin films deposited by sputtering show measure conductivity AC. Indeed, Mahmood [11] obtained with resistivity $10^{11}\Omega$.cm, however, a ZnO target. Inukai [12] succeeded deposit ZnO with a zinc target in an oxygen level of 10% and obtained after annealing, resistivity$10^{12}\Omega$.cm.

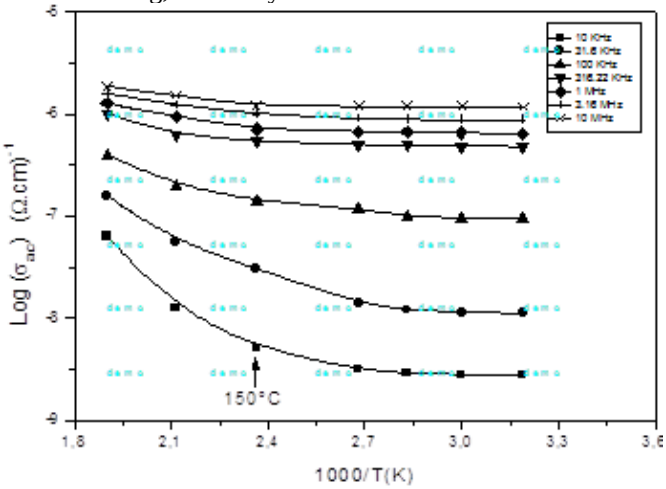


Figure 2: Temperature dependence of the conductivity showing the change in the activation energy

To avoid the phenomenon of space charge to the electrodes, we conducted a study of the conductivity as a function of the inverse temperature for several frequencies characteristic of our study interval (10 kHz - 10 MHz). The fig.2 shows the results.

These curves reveal two distinct phenomena either side of T = 150°C, temperature at which occurs a change in slope. When the temperature exceeds 150°C, the conductivity increases rapidly with temperature and follows a law of approximately Arrhenius type with the activation Ea and k the Boltzmann constant (k = 8,62.10^{-5}eV/K); it is therefore a process of thermally activated conduction. Between 0 and 150°C, the activation energy is equal to 0.09eV. Beyond this threshold of 150°C, the temperature influence is noticeable in this activation energy is 0.22eV and. In the range 40°C - 150°C, the electric conductivity is associated with very low activation energies. This behavior is typical of the hopping conduction between carriers located in various crystalline materials [13] states. Above 150°C the conductivity is independent of frequency but increases rapidly with temperature.

It was due to impurities such as oxygen vacancies which act as acceptor levels located above the valence band [14].

The associated energies are very important. In addition, both sides of the temperature of 150°C, extrapolation of the log curve $\sigma(\omega) = f\left(1/T\right)$ observed in both areas gives an order of magnitude of the energy to activation at 10 KHz.
The measures according to the frequency and temperature performed directly gives both are fundamental electrical characteristics as the relative permittivity $\left(\varepsilon_r = C_p / \varepsilon_0\right)$ and the tangent of the loss angle$\left(\tan\delta = 1/\omega R_p C_p\right)$. We are interested in the influence of frequency and temperature. These measurements were made under the same experimental conditions as the electrical conductivity. Changes in the dielectric constant and loss as a function of frequency at different temperatures are shown respectively in Fig.3 and Fig.4. Dispersions $\tan\delta(\omega,T)$ and $\varepsilon_r(\omega,T)$ are similar to the sample.

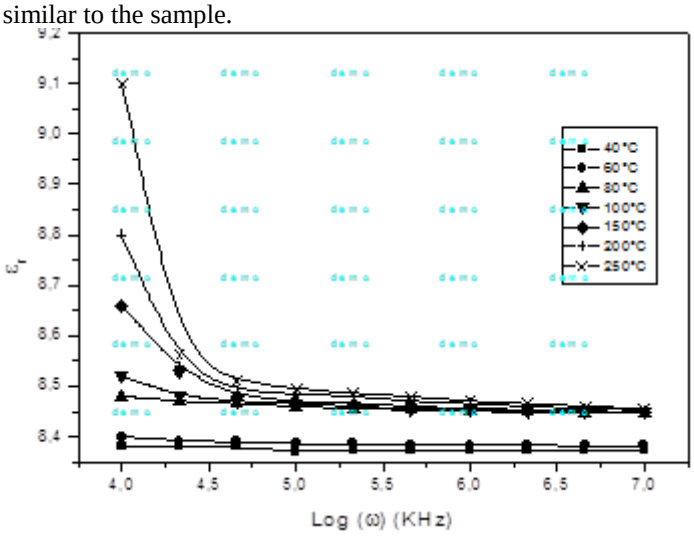


Figure 3: Frequency dependence of ε_r at different temperatures

We note that in Fig.3 dielectric constant varies little at low temperatures and has a significant change to high temperatures (T ≥150°C). We observe that the dielectric constant increases with temperature. In fact, with increasing temperature, a bias is created due to the space charge. This has the effect of giving a measured permittivity exceeds the

Licensed Under Creative Commons Attribution CC BY

real value at low frequency. Permittivity obtained is then apparent.

Fig.4, experimental results of the dielectric loss as a function of frequency at various temperatures show the same behavior as the dielectric constant. We observe, at low temperature, that the dielectric losses are approximately constant as a function of frequency and have a value of about 10^{-4}. At high temperatures, the losses increase with temperature at low frequencies.

The variation of the dielectric constant and loss as a function of frequency at various temperatures shows no relaxation peak. Lack of relaxation peak in the study area is due to the fact that the dielectric losses are low in our sample. Sign of a sample of good quality. Thus, the contribution to the imaginary part of the total permittivity is negligible.

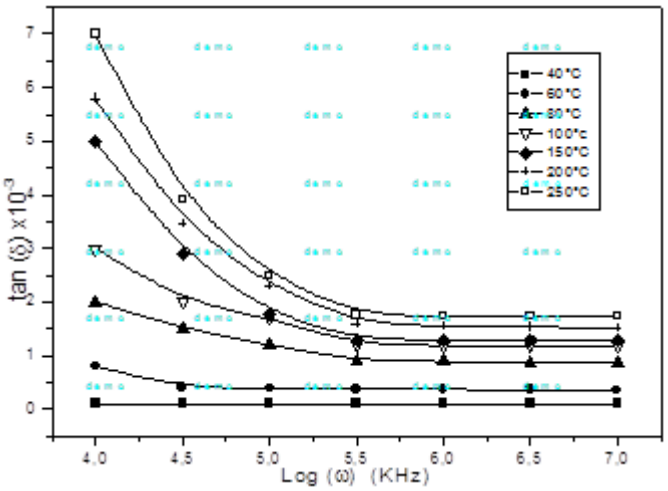


Figure 4: Dielectric losses function of frequency at different temperature.

3.2 Characterization in Microwave

The electrical impedance at the input of the computed from the matrix (6) is [15, 16] structure of fig. 5:

$$Z_e = \frac{1}{jC_0\omega} + \frac{k^2}{C_0\omega} Z_p \frac{2Z_p(\cos(\varphi)-1)+j(Z_1+Z_2)\sin(\varphi)}{Z\,(Z_1+Z_2)\cos(\varphi)+j(Z_p^2+Z_1Z_2)\sin(\varphi)} \quad (6)$$

Z_p, Z_1, Z_2 respectively represents the acoustic impedances of the piezoelectric material, settings on the front and rear of the piezoelectric material. k^2 represents the electromechanical coupling coefficient.

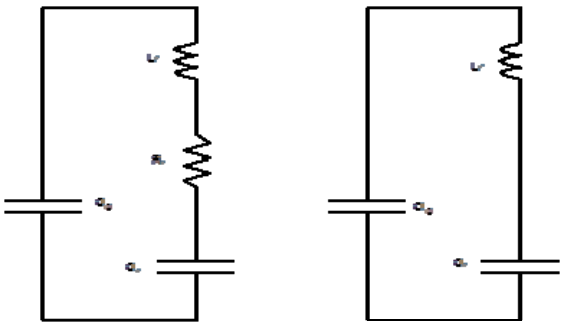


Figure 5: Electrical equivalent circuit of a piezoelectric resonator a) Model of Mason; b) Piezoelectric free

$C_0 = \frac{\varepsilon_r \cdot A}{d}$ is the capacitance of the piezoelectric material and is a constant φ.

To facilitate the study, first look at all the case of a free resonator. The model was developed to account for various losses related to the piezoelectric material [16,17]. We consider, for this, a thin piezoelectric layer, the two sides are metalized, and the electrical impedance is written in this case:

$$Z_e = \frac{1}{jC_0\omega}\left(1+K^2\frac{\tan(\varphi/2)}{\varphi/2}\right) = \frac{1}{jC_0\omega}\left(1+K^2\frac{\tan(\omega d/2V_p)}{\varphi d/2V_p}\right) \quad (7)$$

Around the resonance this resonator can be represented by the following equivalent electric circuit.

C_0 is dielectric capacitance of the ZnO, L_1 represents the inertia of the circuit structure, and the friction losses are R and $C_1$is stiffness of the system. This circuit is an ideal model to represent the physical characteristics of a free resonator.

Indeed, when $\omega \to 0$, the parallel resonance frequency (frequency at which the maximum resistance is R) and series (frequency for which the conductance G is a maximum) of the circuit may be written:

$$f_S = \frac{1}{2\pi\sqrt{L_1C_1}} \text{ et } f_p = \frac{1}{2\pi\sqrt{L_1\frac{C_1C_0}{C_1+C_0}}} \quad (8)$$

The IEEE standard [16] shows that the coupling coefficient k^2 is given by

$$k^2 = \frac{\varphi}{\tan\varphi} \text{ with } \varphi = \frac{\pi}{2}\frac{f_S}{f_p} \quad (9)$$

Formula can be written in a more explicit form and approximate the error introduced by the approximation is then less than 1% in the case where $k^2 < 0.2$, namely:

$$k^2 = \frac{\pi^2}{4}\frac{f_S}{f_p}\left(1-\frac{f_S}{f_p}\right) \quad (10)$$

This means that one can calculate the coupling coefficient k^2 by simply raising the maximum of the real parts of the impedance and admittance, ie, raise the maximum values of the impedance and admittance at the resonant frequency when the imaginary parts are zero.

Using the relation (6), we plotted the theoretical evolution of the real and imaginary parts of the electric admittance of the resonator free, thick 5.7µm, depending on the frequency. Since the modeling was done for the propagation of longitudinal waves of volume, we find a good coupling coefficient k^2 = 7.8%, k = 0.28 for a pure longitudinal mode [15].

The Fig.6 shows the variation of the real and imaginary parts of the electric admittance versus frequency. We observe a change in the electrical input admittance of the resonator and the appearance of the produced oscillations superimposed on the general envelope. These oscillations are due to the propagation medium.

Licensed Under Creative Commons Attribution CC BY

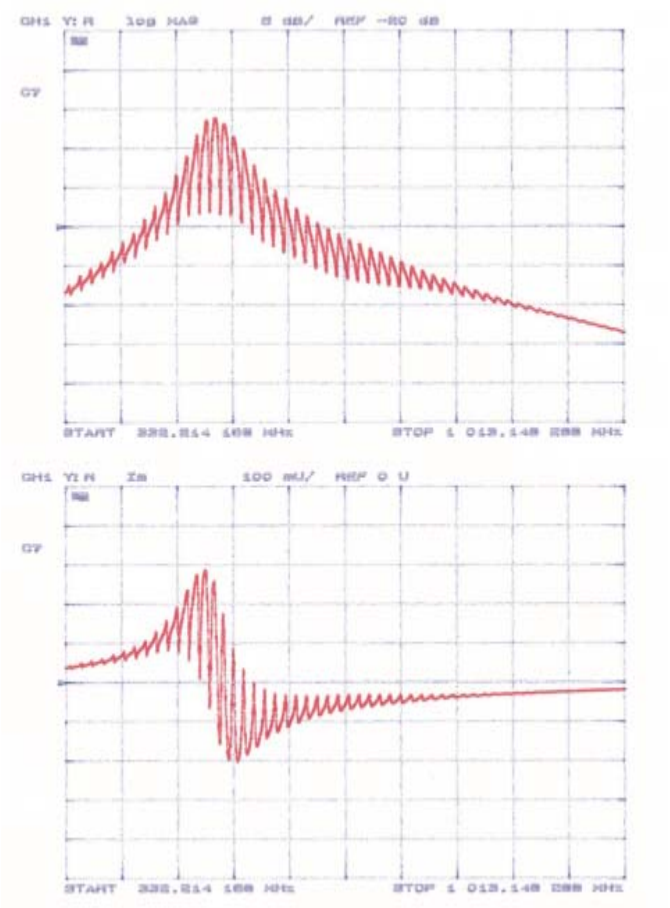


Figure 6: rms of Admittance curves measured on the ZnO based FBAR situated at the center of the wafer as function of frequency.

They reflect changes in real and imaginary parts of the electrical admittance measured. This means that the system reacts to the electrical load with a lag effect. Indeed, the shape of the curves shows that there is interference of waves propagating in the propagation medium which is the silicon substrate. In support of our study, we also measured changes in the reflection coefficient as a function of frequency on a Smith chart. We observe, in Fig.7, the presence of the ZnO piezoelectric activity. To determine the coupling coefficient of our structure, we placed the fundamental resonance of the resonator, ie at frequencies where the real part of the admittance maximum and the minimum susceptance.

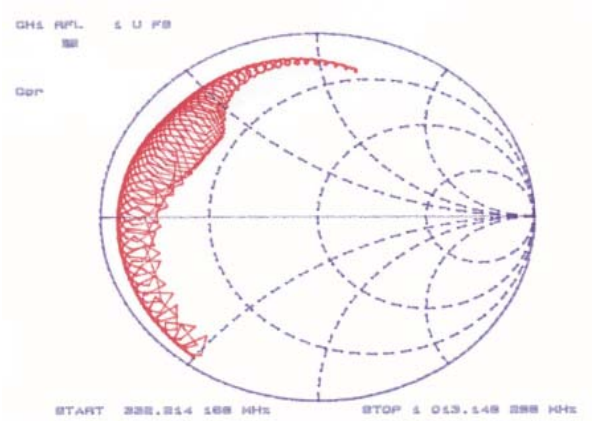


Figure 7: Characteristic of ZnO based FBAR: Smith chart

We performed a piezoelectric resonator using the zinc oxide layer having a resonant frequency of the fundamental mode. The layer of zinc oxide and the delay line are respectively 3.8µm and 380µm thick. The fig.8 shows the evolution of the effective coupling coefficient in k_{eff}^2 versus frequency. We note that the value of the coupling coefficient decreases as the ZnO layer is loaded. ie that there is shift in resonance frequency of the fundamental mode of the structure as and when we load the ZnO. Also the amplitude of the curve decreases with the load. This makes us say that the measured coupling coefficient that is not ZnO but rather that of the entire structure.

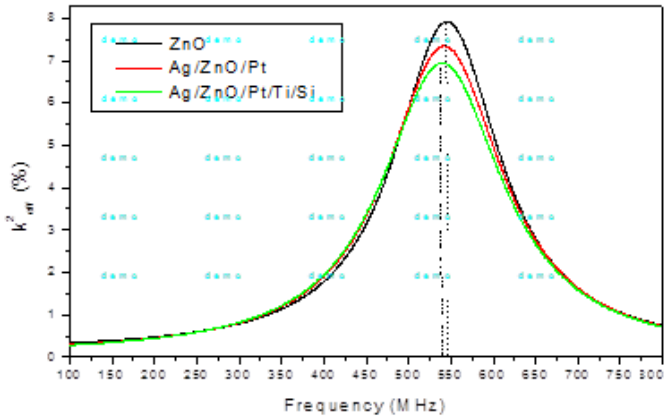


Figure 3: k^2_{eff} distribution coefficient as function of frequency of resonator ZnO

To verify the consistency of the experimental result with the theory on the measurement of the real and imaginary part of the admittance as well as the calculation of the coupling coefficient we considered the delay line as semi-finished. The effective coupling coefficient measured is given in this case by:

$$k^2_{eff}(m) = \frac{\pi^2}{4}\frac{f_s(m)}{f_p(m)}\left[1-\frac{f_s(m)}{f_p(m)}\right] \quad (11)$$

where m is the measure.
From the equation (11), we derive the coupling coefficient of ZnO or

$$k^2_{eff} = \left(1+\frac{\rho_S d_S}{\rho d}\right)\cdot k^2_{ZnO} \quad (12)$$

Given that the maximum electrical admittance occurs for $f_s = 520MHz$ and that the minimum susceptance occurs for $f_p = 537MHz$. Then we get an effective coupling coefficient $k_{eff} = 0.26$ or $k_{ZnO} = 0.255$. We see that the model allows us to show the agreement between the theoretical and experimental results.

Table.2 gives the results obtained by modeling, using the different resonators zinc oxide layer and the results obtained experimentally. We see that the smoothing method allows us to show the good agreement between theoretical and experimental results. This proves that the observation of the variation of the admittance at resonance is a good way to measure the piezoelectric activity of resonant structures.

Licensed Under Creative Commons Attribution CC BY

Table 2: modeling experimentally results using the resonators zinc oxide.

Resonators		G_m (MHz)	B_m (MHz)	k^2_{eff} (%)	k^2_{eff}/k^2_{ta} (%)	k_{eff}
Theory	ZnO	533	555	7,8	99	0,28
	Ag/ZnO/Pt	527	548	7,5	96	0,274
	Ag/ZnO/Pt/Ti/Si	523	543	7,2	92	0,27
Experimentals Results	Ag/ZnO/Pt/Ti/Si (3,8 µm)	520	537	6,94	89	0,264

However, the slip frequency, observed on the experimental result with respect to the theoretical result is probably linked to either the thickness of the ZnO which appears much larger than the measured or the propagation environment value. In effect, the fluctuation of the acoustic impedance of silicon, which is the main cause propagation loss, may be due to the presence of grain boundary silicon.

4. Equations

In conclusion, the best quality ZnO films in terms of crystalline structure have been grown on silicon substrate at power inject 50W employing RF magnetron sputtering method from a metallic zinc target. For high temperatures and low frequencies free-carrier conduction with mean activation energy of approximately 0.3eV was observed. Both the electrical conductivity and the dielectric constant showed a maximum for the ZnO sample deposited at 100°C, explained by crystallographic change according to the previous studies. The dielectric constant is found to be nearly frequency-independent at room temperature. The FBAR devices with the ZnO films exhibited a pronounced resonance peak centered at 537 MHz with a k^2 coupling coefficient of 7 %.

References

[1] J.S. Wang, A.R. Landin, M.M. Lakin, (1983). Low Temperature Coefficient Shear Wave Thin Films for Composite Resonators and Filters, *IEEE Ultrasonics Symposium*, p.491-494.
[2] M.M. Driscoll, A.R. Moore, J.E. Rosebaum, (1986). Recent Advances in Monolithic Film Resonator Technology, *IEEE Ultrasonics Symposium*, p.365-370.
[3] G.R. Kline, M.M. Lakin, (1983). Composite Thin Film UHF Bulk Acoustic Wave Resonators on GaAs. *IEEE Ultrasonics Symposium*, p.495-497.
[4] S. Fujishima, T. Kasanami, T. Nakamura, (1983). Piezoelectric thin films and their applications for electronics. *Jpn. J. Appl. Phys.22*, p.150.
[5] Pinkett SL, Hunt WD, Barber BP, Gammel PL (2002). Determination of ZnO temperature coefficients using thin film bulk acoustic wave resonators. *IEEE Trans Ultrason Ferroelectr Freq Control. Nov, 49(11)*, p.1491.
[6] Frans C. M. Van De Pol, (1990). Thin-Film ZnOiProperties and Applications. *Ceramic Bulletin 69*, p. 1559-1965.
[7] T. Minami, H. Nanto and S. Takata, (1984). Highly conductive and transparent zinc oxide films prepared by rf magnetron sputtering. *J. Appl. Phys. 23*, p. 280.
[8] f. k. shan, g. x. liu, b. i. kim, b. c. shin, s. c. kim and y. s. yu, (2003). Studies of zno thin films on sapphire (0001) substrates deposited by pulsed laser deposition. *j. korean phys. soc.42*, p. 1157.
[9] R. Ondo-Ndong, F. Pascal-Delannoy, A. Boyer, A. Giani, A. Foucaran, (2003). Structural properties of zinc oxide thin films prepared by r. f. magnetron sputtering. *Mat. Sci. Eng. B97*, P. 68-73.
[10] S. R. Elliott, (1977). A theory of a.c. conduction in chalcogenide glasses. *Phil. Mag., 36 (6)* p. 1291-1304.
[11] F. S. Mahmood, R. D. Gould, (1994). A.c. properties of ZnO thin films prepared by r.f. magnetron sputtering. *Thin solid Films 253*, p. 529-533.
[12] T. Inukai, M. Matsuoka, K. Ono, (1995). Characteristics of zinc oxide thin films prepared by r.f. magnetron-mode electron cyclotron resonance sputtering. Thin Solid Films 257, p. 22-27.
[13] H. Scher and M. (1973). Stochastic Transport in a Disordered Solid. II. Impurity Conduction Lax, *Phys. Rev., 7 (10)* p. 4502.
[14] R. D. Gould, A. K. Hasan, (1993). A.c. electrical properties of thermally evaporated thin films of copper phthalocyanine. Thin Solid Films 223, p. 334-340.
[15] D. Royer, E. Dieulesaint, « Ondes élastiques dans les solides », Tome 2, ed. Masson (1996).
[16] IEEE standard on piezoelectric IEEE / ANSI std. 176 (1987).
[17] Zhang, Z. Wang, J. D. N. Cheeke, (2000). Simulation of electromechanical coupling coefficient by modified modal frequency spectrum method including the electrode effect. Ultrasonics 38, p.114-117.

Licensed Under Creative Commons Attribution CC BY